Avalanches and force drops in displacement-driven compression of porous glasses

Víctor Navas-Portella,[1,2] Álvaro Corral,[1,3] and Eduard Vives[2]
[1]*Centre de Recerca Matemàtica, Edifici C, Campus Bellaterra, E-08193 Bellaterra, Catalonia, Spain*
[2]*Departament de Matèria Condensada, Facultat de Física, Universitat de Barcelona, Diagonal 645, 08028 Barcelona, Catalonia, Spain*
[3]*Departament de Matemàtiques, Universitat Autònoma de Barcelona, Cerdanyola, Catalonia, Spain*
(Received 29 July 2016; published 30 September 2016)

Similarities between force-driven compression experiments of porous materials and earthquakes have been recently proposed. In this paper, we measure the acoustic emission during displacement-driven compression of a porous glass. The energy of acoustic-emission events shows that the failure process exhibits avalanche scale-invariance and therefore follows the Gutenberg-Richter law. The resulting exponents do not exhibit significant differences with respect the force-driven case. Furthermore, the force exhibits an avalanche-type behavior for which the force drops are power-law distributed and correlated with the acoustic emission events.

DOI: 10.1103/PhysRevE.94.033005

I. INTRODUCTION

Earthquakes constitute a complex phenomenon which has been studied for a long time due to their impact as natural disasters. From a fundamental point of view, statistical laws in seismology have attracted the attention not only of geoscientists but also of physicists and mathematicians due to their signs of scale invariance. Recent works have found that some of these laws also manifest in materials which exhibit crackling noise: porous glasses [1,2], minerals [3] and wood under compression [4], breaking of bamboo sticks [5], ethanol-dampened charcoal [6], confined-granular matter under continuous shear [7], etc. Due to the difference between time, space, and energy scales, these analogies have sparked important interest in the condensed-matter-physics community. In general, the experimental results are based on the analysis of acoustic emission (AE) signals in the ultrasonic range, which are detected when these systems are mechanically perturbed.

Baró *et al.* [2,3] found statistical similarities between earthquakes and the AE during compression experiments of porous materials. In that case, the experiments were performed using the applied force as a driving parameter, which means that the force increases linearly in time (force-driven compression). Crackling noise during failure of porous materials has also been studied through computational models that show qualitative agreement with experimental results [8,9]. Within the context of structural phase transitions, it has been shown that avalanche scale-invariance manifests in different ways depending on the driving mechanism [10]. If the control variable for the driving is a generalized force, disorder plays an important role leading to a dominant nucleation process, and the criticality is of the order-disorder type. However, if the driving mechanism consists in the control of a generalized displacement, the critical state is reached independently of the disorder and by means of a self-organized criticality mechanism. These results were experimentally confirmed [11,12] based on the study of amplitude and energy distributions in AE experiments of martensitic transformations. The influence of the driving mechanism has been studied in the slip events occurring in compressed microcrystals [13]. One question that still holds is whether the driving mechanism will influence the distributions of AE events in the case of failure under compression experiments. This question is important because when comparing with earthquakes, the natural accepted mechanism is that tectonic plates are driven at constant velocity at far enough distances from the faults [14]. Here we study the displacement-driven compression of porous glasses with the aim of answering this question.

When changing the driving mechanism from force to displacement, the first main macroscopic difference is that force fluctuates and shows drops that, as will be shown, correlate with AE events. Recently, Illa *et al.* have shown that the driving mechanism influences the nucleation process in martensitic transformations and these microscopic effects can lead to macroscopic changes in stress-strain curves in which force fluctuations appear [15]. An exponentially truncated power-law distribution has been found for torque drops in shear experiments of granular matter [7]. Serrations or force drops have also been studied in metallic single crystals [16], metallic glasses [17–19], and high-entropy alloys [20]. These studies are essentially focused on the presence of criticality. Furthermore, Dalla Torre *et al.* studied the AE during the compression of metallic glasses and concluded that there exists a correlation between AE bursts and stress drops [19]. In this work we provide a description of the distribution of force drops in displacement-driven compression experiments of porous glasses and a correlation between these force drops and the energy of the recorded AE events is identified.

The paper is structured as follows: in Sec. II the experimental methods as well as the sample details are described. Results are analyzed in Sec. III, which is divided in three subsections: the first one (III A) refers to the study of AE events, the second one (III B) focuses in the study of force drops, and the third one (III C) is devoted to the study of the relation between the energy of AE events and force drops. A brief summary and the conclusions are reported in Sec. IV.

II. EXPERIMENTAL METHODS

Uniaxial compression experiments of porous glass Vycor (a mesoporous silica ceramics with 40% porosity) are performed in a conventional test machine ZMART.PRO (Zwick/Roell). The cylindrical samples, with diameters Φ of 1 mm and

2 mm and different heights H, are placed between two plates that approach each other at a certain constant compression rate $\dot{z}$. We refer to such framework as displacement-driven compression. Compression is done in the axial direction of the cylindrical samples with no lateral confinement. The force opposed by the material is measured by means of a load cell Xforce P (Zwick/Roell), with a maximal nominal force of 5 kN and output to a communication channel every $\Delta t = 0.1$ s. Performing blank measurements in the same conditions as those of the experiments presented below, we have checked that force uncertainties are of the order of 10^{-2} N. Simultaneous recording of AE signals is performed by using piezoelectric transducers embedded in both plates. The electric signals are preamplified (60 dB), band filtered (between 20 kHz and 2 MHz), and analyzed by means of a PCI-2 acquisition system from Euro Physical Acoustics (Mistras Group) working at 40 MSPS. The AE acquisition system also reads the force measured by the conventional test machine through the communication channel. Recording of the data stops when a big failure event occurs, the sample gets destroyed, and the force drops to zero.

We prescribe that an AE avalanche or event starts at the time t_i when the preamplified signal $V(t)$ crosses a fixed threshold of 23 dB, and finishes at time $t_i + \Delta_i$ when the signal remains below threshold from $t_i + \Delta_i$ to at least $t_i + \Delta_i + 200\mu$s. The energy E_i of each signal is determined as the integral of $V^2(t)$ for the duration Δ_i of the event divided by a reference resistance of 10 kΩ.

Different experiments have been performed at room temperature for 13 different Vycor cylinders with different diameters and heights as well as different compression rates. We have checked that different cleaning protocols before the experiment do not alter the results. All the details related to experiments are listed in Table I. Figure 1 shows a typical experimental output for the sample V12. Panel (a) displays the sequence of energies of the AE events and the evolution of the force as a function of the time. The acoustic activity rate r (s^{-1}) has been computed as the number of events per unite time recorded along windows of 20 s. Its behavior is shown in Fig. 1(b) together with the cumulative number of events as a function of the time. It must be noticed that force drops occur along the whole curve and clearly show variability on three to four orders of magnitude. In general, the largest force drops coincide with AE events with very large energy.

TABLE I. Summary of dimensions and compression rates $\dot{z}$ for the different experiments reported in this work.

Sample	Φ(mm)	H(mm)	$\dot{z}$ (mm/min)
V105	1	0.5	2×10^{-3}
V11	1	1	2×10^{-3}
V115	1	1.5	2×10^{-3}
V12	1	2	2×10^{-3}
V125	1	2.5	2×10^{-3}
V205	2	0.5	1×10^{-2}
V21	2	1	1×10^{-2}
V22	2	2	1×10^{-2}
V23	2	3	1×10^{-2}
V26	2	6	1×10^{-2}
V28	2	8	1×10^{-2}
V212	2	12	1×10^{-2}
V24	2	4	5×10^{-2}

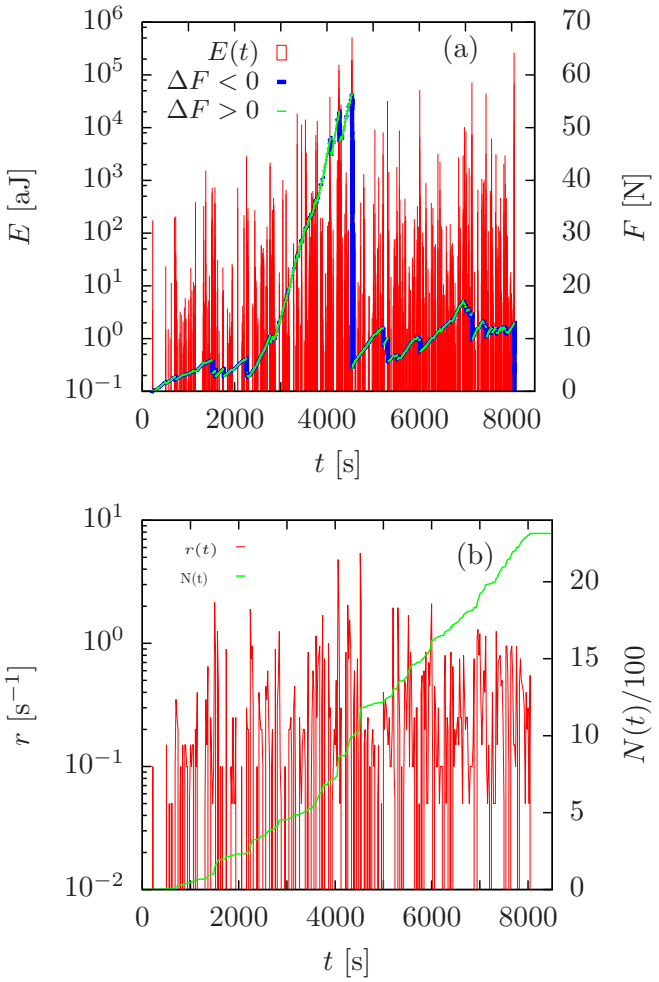

FIG. 1. Typical output for the sample V12. (a) The energy of the AE events as well as the measure of the force as a function of time. Green lines represent those time intervals ($\Delta t = 0.1$ s) in which the force increases whereas blue lines represent those for which the force decreases (force drops). (b) The activity rate of the experiment as well as the cumulative number of AE events $N(t)$ as a function of time.

III. RESULTS

A. Acoustic emission data

In force-driven compression experiments of porous glasses [1,2] it was found that the energy probability density $P(E)$ of AE events follows a power law with exponent $\epsilon = 1.39 \pm 0.05$ independently of the loading rate (0.2–12.2 kPa/s),

$$P(E)dE = (\epsilon - 1)E_{\min}^{\epsilon-1}E^{-\epsilon}dE, \quad (1)$$

where $E_{\min} \sim 1$ aJ is the lower bound required for the normalization of the probability density. Figure 2(a) shows an example of histogram of the energy of AE events for the

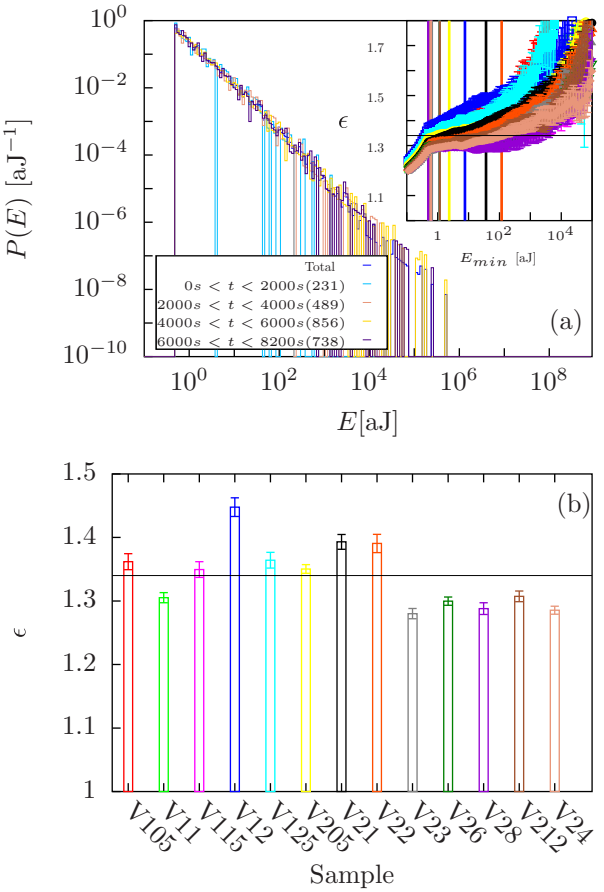

FIG. 2. (a) The energy distribution for the sample V12 for different time windows as well as for the whole experiment. The numbers in parentheses account for the number of AE events in each time interval. Inset presents the MLE of the exponent ϵ as a function of the lower threshold $E_{\min}$ for all the samples. Vertical lines correspond to the fitted values of $E_{\min}$ and ϵ. The color code for each sample can be read from the color bars in panel (b). (b) The value of the exponent ϵ is shown for each sample. The dark horizontal line in the inset and in (b) is the mean value of the exponent $\epsilon = 1.34$.

sample V12 in one of our displacement-driven experiments. As can be seen, data seem to follow the Gutenberg-Richter law for more than six decades. The different curves, corresponding to consecutive time windows of approximately 2000 s, reveal that the energy distribution is stationary.

We use the procedure exposed in Ref. [21] in order to guarantee statistical significance in the fit of the exponent ϵ and the lower threshold $E_{\min}$. Considering as a null hypothesis that the energy distribution follows a nontruncated power law [see Eq. (1)], maximum likelihood estimation (MLE) for the exponent ϵ is computed for increasing values of the lower threshold $E_{\min}$ (see inset of Fig. 2). For each lower threshold and its corresponding exponent, a Kolmogorov-Smirnov test of the fit is performed with a resulting p value. The final values of the exponent and the threshold are chosen once the p value has first overcome the significance level $p_c = 0.05$ and the power-law hypothesis cannot be rejected. The obtained values for every sample are shown in Fig. 2(b) together with the standard deviation of the MLE. The horizontal lines in

TABLE II. Number of AE events N_{AE}, number of those which are power-law distributed $N_{\mathrm{AE}}^{\mathrm{PL}}$, value of the lower threshold $E_{\min}$, maximum value E_{Max}, and exponent ϵ. The standard deviation of the MLE is of the order of 10^{-2}.

Sample	N_{AE}	$N_{\mathrm{AE}}^{\mathrm{PL}}$	$E_{\min}$ [aJ]	E_{Max} [aJ]	ϵ
V105	869	829	0.602	1.84×10^5	1.36
V11	1438	1438	0.502	2.69×10^6	1.31
V115	836	797	0.626	1.10×10^6	1.35
V12	2314	928	7.669	5.16×10^5	1.45
V125	1097	865	1.128	4.94×10^5	1.36
V205	4160	2609	2.361	9.97×10^6	1.35
V21	4170	1136	36.707	1.07×10^7	1.39
V22	3683	746	117.583	6.57×10^6	1.39
V23	1275	1196	0.645	7.16×10^6	1.28
V26	2071	2065	0.516	1.38×10^7	1.30
V28	974	974	0.501	2.82×10^6	1.29
V212	1646	1338	1.15	4.37×10^6	1.31
V24	2129	2039	0.595	5.97×10^6	1.29

Fig. 2(b) and in the inset of Fig. 2(a) show the average value and associated standard deviation $\epsilon = 1.34 \pm 0.03$. In spite of the variations around this mean value, it seems that the value of the exponent does not have a strong dependence neither on the dimensions of the sample nor on the compression rate. Complementary information obtained from the fitting method is presented in Table II.

The average value of the exponent $\epsilon = 1.34 \pm 0.03$ found for the present displacement-driven experiments is compatible with the value found in force-driven measurements $\epsilon = 1.39 \pm 0.05$. Contrarily to what happens in martensitic transformations [12], we conclude that there are no clear evidences that the driving mechanism changes the value of the exponent in compression experiments.

B. Force drops

The evolution of the force as a function of time is shown in Fig. 1. We define force changes as $\Delta F(t) = -(F(t + \Delta t) - F(t))$, with $\Delta t = 0.1$ s, so that force drops are positive. As can be observed in Figs. 3(a)–3(c) the distribution of ΔF can exhibit several contributions. There is a clear Gaussian-like peak corresponding to negative ΔF that shifts to the left when increasing the compression rate. This peak is related to the average elastic behavior of the porous material. The rest of the contributions in the negative part of the histogram correspond to the different elastic regimes of the material as it experiences successive failures.

In the present work we will only focus on the positive part of this distribution which corresponds to the force drops. Our goal is to find whether the distribution of force drops is fat-tailed or not. In Figs. 4(a)–4(c) the distribution of force drops ($\Delta F > 0$) corresponding to Fig. 3 is shown in log-log scale. For completeness, complementary cumulative distribution functions or survivor functions $S(\Delta F)$ are also shown in Figs. 5(a)–5(c). The probability density of force drops seems to follow a power law $D(\Delta F) \propto \Delta F^{-\phi}$ which holds for three decades in the case of the slower compression rate and four decades for the higher ones. This difference is

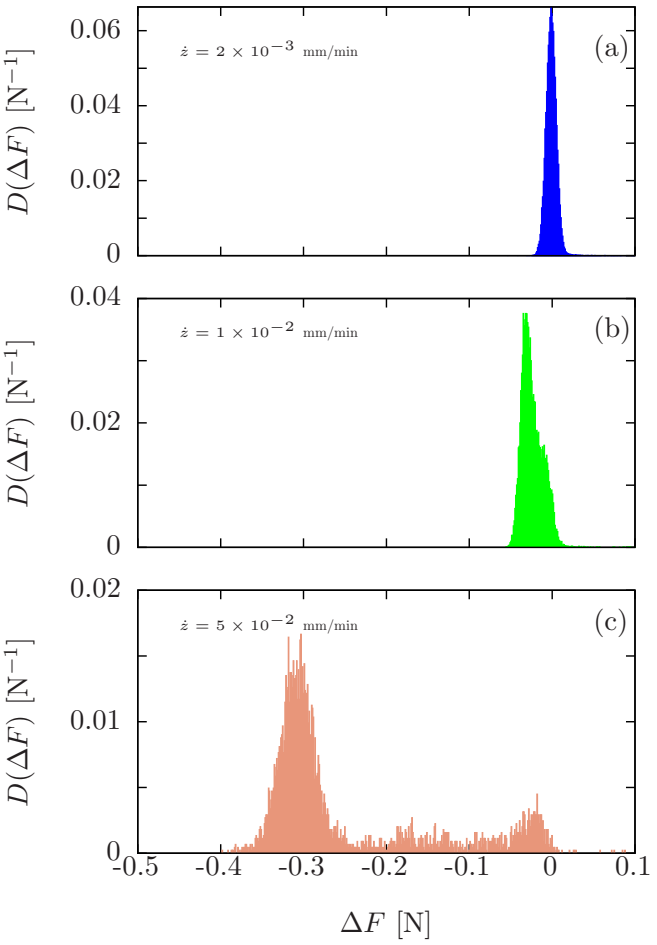

FIG. 3. Probability densities of ΔF for three samples with different compression rates. Sample V12 compressed at $\dot{z} = 2 \times 10^{-3}$ mm/min is shown in (a), sample V212 compressed at $\dot{z} = 1 \times 10^{-2}$ mm/min in (b), and sample V24 compressed $\dot{z} = 5 \times 10^{-2}$ mm/min is presented in (c).

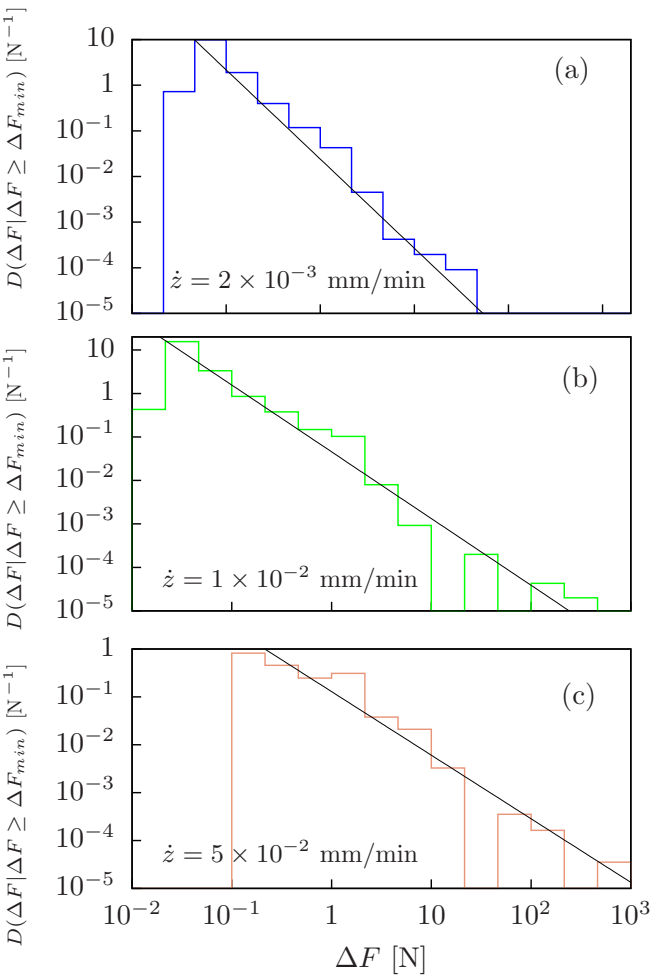

FIG. 4. Probability densities of force drops ΔF and their corresponding fits for V12 (a), V212 (b), and V24 (c). Distributions are displayed and normalized for $\Delta F \geqslant \Delta F_{\text{min}}$.

essentially due to the difference of surfaces of samples. The larger the surface contact between the sample and the plate, the larger the force opposed by the material. Note that, in contrast to Fig. 3, the distribution of ΔF is conditioned to ΔF larger or equal than the lower threshold ΔF_{min} obtained from the fit.

In order to determine from which value ΔF_{min} the power-law hypothesis holds, the fit of the right tail of the distribution of ΔF has been performed following the same procedure as that followed for the energy distribution. In Figs. 6(a)–6(c) MLEs of the exponent ϕ as a function of the lower threshold for the samples compressed at different compression rates are shown. Three samples have been excluded due to wrong sampling of the measurement of the force. Vertical lines of different colors represent the selected threshold ΔF_{min} for each sample. Note that, contrarily to what happens in the MLE of the energy exponent, for the lowest values of ΔF_{min} where the power-law hypothesis is not already valid, there is an overestimation of the exponent due to the presence of the Gaussian peak.

The value of the exponents ϕ for the different samples is shown in Fig. 6(d), and three clear groups can be distinguished. The value of the exponent is higher for the slower compression rate and decreases for increasing compression rates. The exponent values are robust under the change of time window Δt. Additional parameters resulting from fits are shown in Table III.

TABLE III. Total number of force drops D_{Tot} and the resulting values of the number of those data which are power-law distributed D_{PL}, values of the lower threshold ΔF_{min} and the value of the largest force drop ΔF_{Max} and the fitted exponent ϕ. The standard deviation of the MLE is around 0.05.

Sample	D_{Tot}	D_{PL}	ΔF_{min} [N]	ΔF_{Max} [N]	ϕ
V115	9960	174	1.73×10^{-2}	8.31	1.79
V12	32 323	445	2.12×10^{-2}	27.61	1.95
V125	26 104	208	1.93×10^{-2}	24.31	1.80
V205	5603	334	3.55×10^{-2}	853.36	1.53
V21	10 787	149	0.16	977.78	1.72
V22	6609	133	9.05×10^{-2}	801.63	1.57
V23	9987	162	1.61×10^{-2}	593.19	1.46
V28	8881	113	1.72×10^{-2}	340.22	1.53
V212	9030	202	1.45×10^{-2}	247.56	1.55
V24	3742	53	5.80×10^{-2}	797.63	1.32

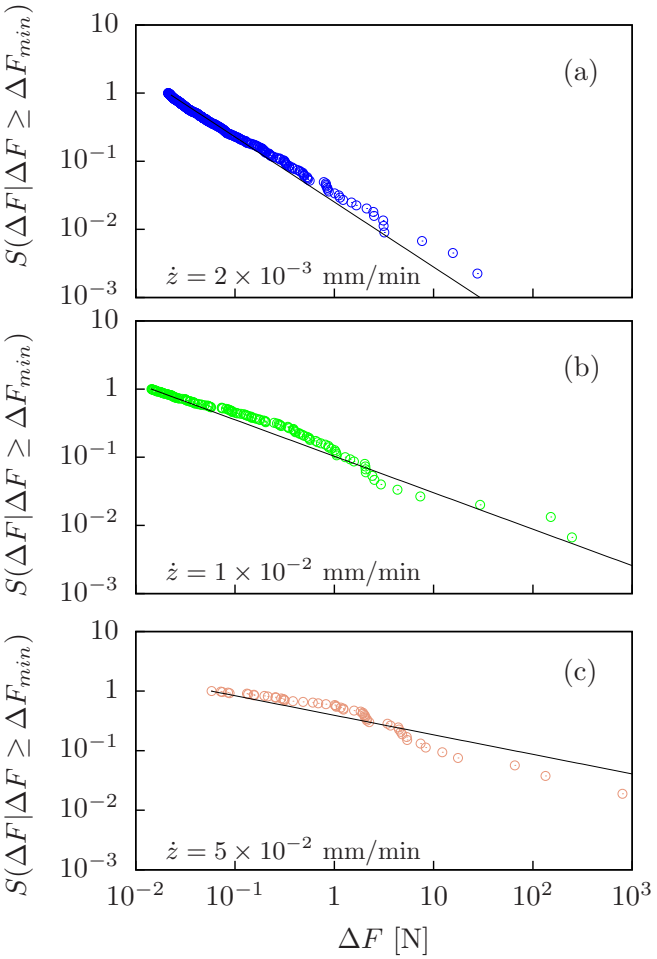

FIG. 5. Survivor functions $S(\Delta F|\Delta F \geqslant \Delta F_{\min})$ and their corresponding fits for V12 (a), V212 (b), and V24 (c). Survivor functions are displayed and normalized for $\Delta F \geqslant \Delta F_{\min}$.

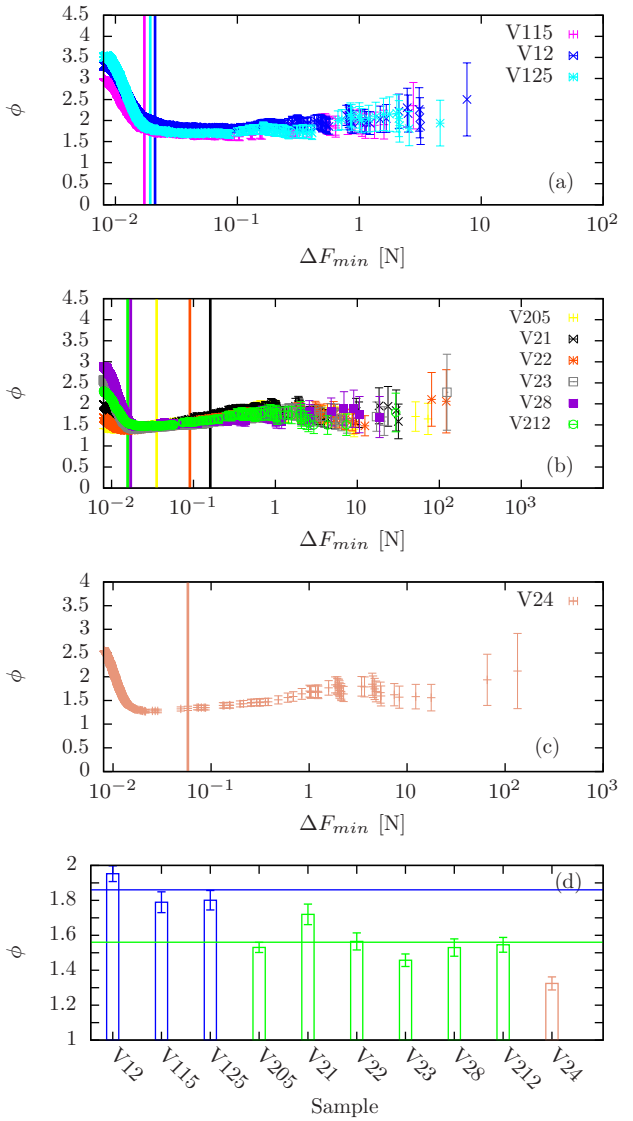

FIG. 6. (a)–(c) The MLE of the exponent ϕ as a function of the lower threshold $\Delta F_{\min}$ for samples compressed at $\dot{z} = 2 \times 10^{-3}$ mm/min, $\dot{z} = 10^{-2}$ mm/min, and $\dot{z} = 5 \times 10^{-2}$ mm/min. Vertical lines in each panel mark the threshold $\Delta F_{\min}$, which is selected by the fitting and testing procedure. (d) The values of the exponent for each sample. Blue horizontal line at 1.85 and green horizontal line at 1.54 are the mean values of the exponent for the two smallest compression rates.

With the use of these techniques, there is evidence that force drops are power-law distributed, as found for metallic glasses [18], with a robust exponent under the change of time window and that decreases for increasing compression rates.

C. Joint distribution of energy and force drops

In this subsection we try to unveil the relation between force drops and the energy of AE events. As can be appreciated in Fig. 1(a), the largest force drops correspond with the highest energy of AE events. Actually, Dalla Torre *et al.* [19] found that there exists a correlation between force drops and AE events, but no evidence of correlation between the amplitude of these signals and the magnitude of the force drops was found. Nevertheless, the energy could show a certain correlation since not only the amplitude plays an important role in its calculation but also the duration of the AE events.

This correlation would be interesting for two reasons: on the one hand, it would set a relation between the energy of AE events, which is from microscopic nature (aJ), and force drops, which are at the macroscopic scale (N). On the other hand, force drops appear every time there is a microfailure in the sample, and thus they can be understood as releases of elastic energy. In the same way as Ref. [19], we find that there is a correlation in time between the occurrence of force drops and the presence of AE events.

In order to associate a certain energy to the ith force drop, we define the quantity

$$W_{D,i}^{\Delta t} = \sum_{j=1}^{N_{\mathrm{AE}}^{i}} E_j, \tag{2}$$

where N_{AE}^{i} is the number of AE events that occur within the time interval of duration $\Delta t = 0.1$ s where the ith force drop appears and E_j is the energy of those AE events. The

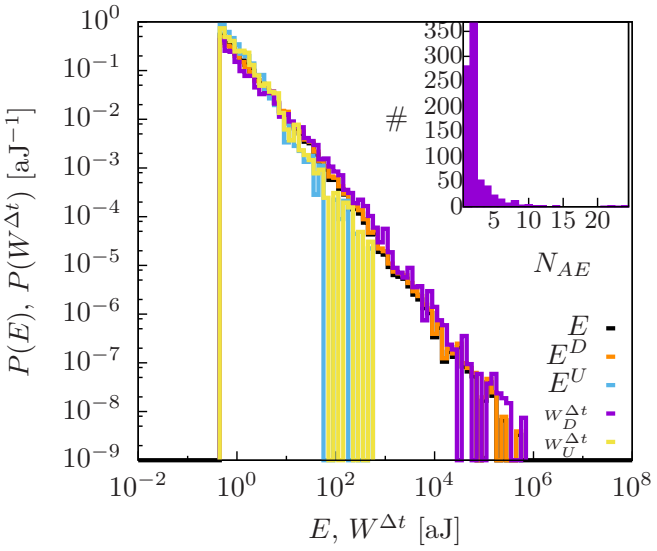

FIG. 7. Main panel shows the distribution of E, the distributions of energies E^D and E^U that appear when a force drop or a force rises occurs, and the distributions of $W_D^{\Delta t}$ and $W_U^{\Delta t}$, which refer to the sum of AE energies for a certain force drop or force rise. The inset represents the histogram of the number of AE events encapsulated in time intervals where force drops occur. All these distributions correspond to the sample V12.

same construction can be done for force increases by defining $W_U^{\Delta t}$. This construction is divided in two steps: the first one consists in splitting the time axis in intervals of duration Δt so that there is a correspondence between AE events and force rises or drops. The second step consists in applying Eq. (2) and its counterpart for $W_U^{\Delta t}$ for every interval with AE events. In Fig. 7(a) we present the different distributions involved in this construction for the sample V12. There are two random variables corresponding to the first step of the transformation: E^D corresponds to the energy when a force drop appears, whereas E^U corresponds to the energy when force rises appear. The second step of the transformation is reflected in the quantities $W_D^{\Delta t}$ and $W_U^{\Delta t}$, which correspond to the sum of energies in every force drop and in every force rise, respectively. The plot in Fig. 7(a) reinforces the importance of the relation between force drops and AE events since the distributions of E^U and $W_U^{\Delta t}$ are restricted to low values of the energy, whereas the range of the distributions of E^D and $W_D^{\Delta t}$ is very similar to the original one. The inset shows the histogram of the number $N_{\rm AE}$ of AE events encapsulated in time intervals of Δt in which there are force drops for the sample V12. The maximum of this histogram is at $N_{\rm AE} = 2$ and decreases up to the maximum encapsulation of $N_{\rm AE} = 24$.

The numbers involved in these constructions are shown for all the samples in Table IV. The fact that there are force rises associated to acoustic emission activity can be explained by the presence of force drops that have not been identified in a Δt interval where the force has globally increased. This prediction agrees with the fact that the energy associated to

TABLE IV. Numbers which are involved in the construction of $W^{\Delta t}$. $U_{\rm Tot}$ and $D_{\rm Tot}$ are the total number of intervals where the force has raised up or dropped. $U_{\rm AE}$ and $D_{\rm AE}$ are the number of force rises and drops with AE events. $N_{\rm AE}$ is the total number of AE events, $N_{\rm AE}^U$ and $N_{\rm AE}^D$ are the number of AE events associated to rises and drops of the force, respectively.

Sample	$U_{\rm Tot}$	$D_{\rm Tot}$	$U_{\rm AE}$	$D_{\rm AE}$	$N_{\rm AE}$	$N_{\rm AE}^U$	$N_{\rm AE}^D$
V115	20 119	9960	119	217	836	191	645
V12	47 663	32 323	251	820	2314	345	1969
V125	37 028	26 104	141	313	1097	215	882
V205	26 564	5603	1028	336	4160	2093	2067
V21	32 380	10 787	1324	223	4170	2572	1598
V22	24 388	6609	930	177	3683	2066	1617
V23	24 922	9987	423	70	1275	804	471
V28	25 468	8881	359	83	974	638	336
V212	27 367	9030	453	135	1646	882	764
V24	8114	3742	602	41	2129	1745	384

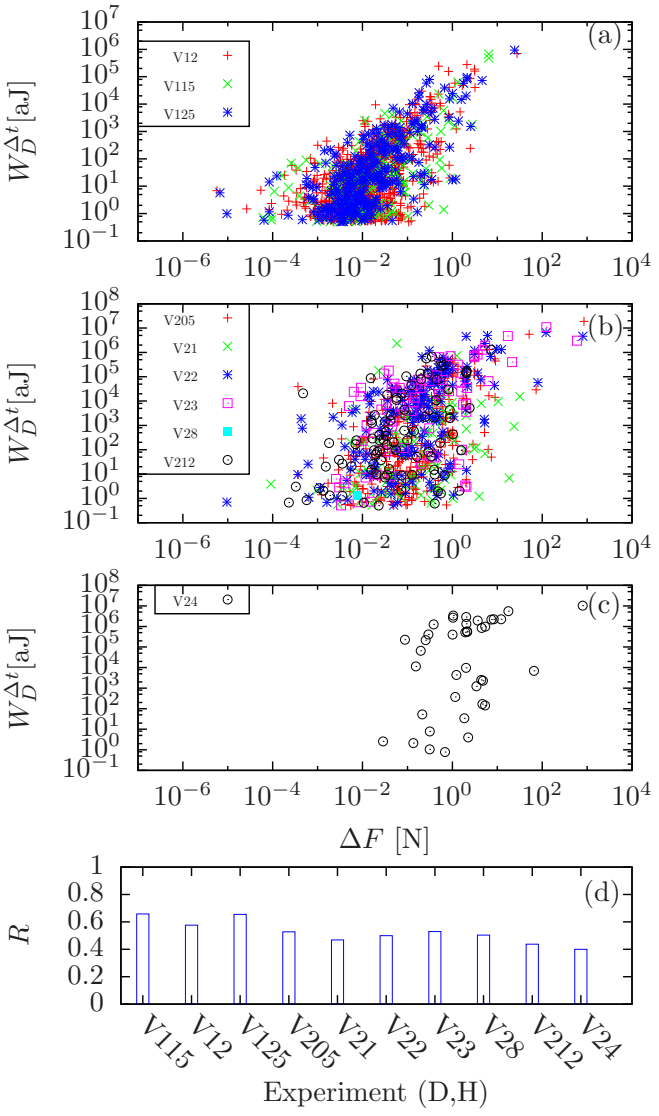

FIG. 8. Scatter plots of the energy released in each force drop for all the samples compressed at $\dot{z} = 2 \times 10^{-3}$ mm/min (a), at $\dot{z} = 10^{-2}$ mm/min (b), and at $\dot{z} = 5 \times 10^{-2}$ mm/min (c). (d) The Pearson correlation for the logarithm of the variables for all the samples.

force rises covers a small range corresponding to low-energy values of the total energy distribution. It is important to remark that, despite the fraction of AE events associated to force drops decreases as the compression rate increases, the fraction that accounts for the average number of events encapsulated in a force drop ($N^D_{\rm AE}/D_{\rm AE}$) is always larger than the average number of AE events encapsulated in intervals where the force is increasing ($N^U_{\rm AE}/U_{\rm AE}$). Hence, increments of AE activity are essentially associated to drops in the force. The total duration of the experiment is given by $T = (U_{\rm Tot} + D_{\rm Tot})\Delta t$. Note that, despite the big difference between the total number of force drops ($D_{\rm Tot}$) and the number of force drops with AE activity ($D_{\rm AE}$), this second number is in the same order of magnitude as the number of power-law data in Table III but larger always. In Fig. 8 we present scatter plots for the different compression rates. It must be noticed that the largest AE events are manifested in those force drops which are power-law distributed. The associated energy of the remaining force drops is relatively low compared with those with large values of ΔF. The rest of force drops that have no associated AE activity are related to experimental fluctuations of the measurement. Under these circumstances, we study the energy associated to force drops and try to unveil if there exists any correlation between them. It must be mentioned that, as has been seen in the previous section, the range of interest of force drops is restricted to those values which exceed 10^{-2} N. In Fig. 8(d) the Pearson correlation of the logarithm of the variables for the range of interest is shown for each sample. These correlations are much higher than the ones resulting after the reshuffling of the data, so they have statistical significance. The correlation is positive, and it establishes a relation between AE events, which are of microscopic nature, with a magnitude of macroscopic character, the force drops.

IV. CONCLUSIONS

In this paper we have reported the results of displacement-driven compression experiments of several Vycor cylinders with different dimensions and different compression rates. The Gutenberg-Richter law is found for the energy distribution in the same way it was previously found for force-driven compression experiments. Regarding the values of the exponents, we conclude that they do not seem to be affected by the driving mechanism in compression experiments. The independence with the driving mechanism has also been found in the measurement of slip events in microcrystals [13].

When the driving variable turns out to be the displacement, the release of elastic energy is not only expressed by means of AE, but it is also manifested as drops in the force which are power-law distributed with a compression-rate-dependent exponent. These drops can also be observed in computer simulations near the big failure event [8,9]. Nevertheless, some tuning of the disorder should be arranged in simulations in order to replicate a situation with a similar level of heterogeneity as in our experiments. Furthermore, we have established a correlation between force drops and the associated energy of AE events.

ACKNOWLEDGMENTS

We thank Jordi Baró and Ferenc Kun for fruitful discussions. The research leading to these results has received funding from "La Caixa" Foundation. Financial support was received from projects FIS2012-31324, FIS2015-71851-P, MAT2013-40590-P, and MAT2015-69-777-REDT (Ministerio de Economía y Competitividad, Spain) and 2014SGR-1307 from Agencia de gestió d'Ajuts Universitaris i de Recerca (AGAUR).

[1] E. K. Salje, D. E. Soto-Parra, A. Planes, E. Vives, M. Reinecker, and W. Schranz, Philos. Mag. Lett. **91**, 554 (2011).
[2] J. Baró, Á. Corral, X. Illa, A. Planes, E. K. H. Salje, W. Schranz, D. E. Soto-Parra, and E. Vives, Phys. Rev. Lett. **110**, 088702 (2013).
[3] G. F. Nataf, P. O. Castillo-Villa, J. Baró, X. Illa, E. Vives, A. Planes, and E. K. H. Salje, Phys. Rev. E **90**, 022405 (2014).
[4] T. Makinen, A. Miksic, M. Ovaska, and M. J. Alava, Phys. Rev. Lett. **115**, 055501 (2015).
[5] S.-T. Tsai, L.-M. Wang, P. Huang, Z. Yang, C.-D. Chang, and T.-M. Hong, Phys. Rev. Lett. **116**, 035501 (2016).
[6] H. V. Ribeiro, L. S. Costa, L. G. A. Alves, P. A. Santoro, S. Picoli, E. K. Lenzi, and R. S. Mendes, Phys. Rev. Lett. **115**, 025503 (2015).
[7] S. Lherminier, R. Planet, G. Simon, K. J. Måløy, L. Vanel, and O. Ramos, Rev. Cub. Fis. **33**, 55 (2016).
[8] F. Kun, I. Varga, S. Lennartz-Sassinek, and I. G. Main, Phys. Rev. E **88**, 062207 (2013).
[9] F. Kun, I. Varga, S. Lennartz-Sassinek, and I. G. Main, Phys. Rev. Lett. **112**, 065501 (2014).
[10] F.-J. Pérez-Reche, L. Truskinovsky, and G. Zanzotto, Phys. Rev. Lett. **101**, 230601 (2008).
[11] E. Vives, D. Soto-Parra, L. Mañosa, R. Romero, and A. Planes, Phys. Rev. B **80**, 180101 (2009).
[12] A. Planes, L. Mañosa, and E. Vives, J. Alloys Compd. **577**, S699 (2013).
[13] R. Maaß, M. Wraith, J. T. Uhl, J. R. Greer, and K. A. Dahmen, Phys. Rev. E **91**, 042403 (2015).
[14] K. M. Larson, J. T. Freymueller, and S. Philipsen, J. Geophys. Res. Solid Earth **102**, 9961 (1997).
[15] X. Illa, P. Winkelmayer, and E. Vives, Phys. Rev. B **92**, 184107 (2015).
[16] M. A. Lebyodkin, Y. Brechet, Y. Estrin, and L. P. Kubin, Phys. Rev. Lett. **74**, 4758 (1995).
[17] J. Antonaglia, X. Xie, G. Schwarz, M. Wraith, J. Qiao, Y. Zhang, P. K. Liaw, J. T. Uhl, K. A. Dahmen, A. Peker, and Johnson, Sci. Rep. **4**, 2342 (2014).
[18] B. A. Sun, H. B. Yu, W. Jiao, H. Y. Bai, D. Q. Zhao, and W. H. Wang, Phys. Rev. Lett. **105**, 035501 (2010).
[19] F. H. Dalla Torre, D. Klaumünzer, R. Maaß, and J. F. Löffler, Acta Mater. **58**, 3742 (2010).
[20] R. Carroll, C. Lee, C.-W. Tsai, J.-W. Yeh, J. Antonaglia, B. A. W. Brinkman, M. LeBlanc, X. Xie, S. Chen, P. K. Liaw, and K. A. Dahmen, Sci. Rep. **5**, 16997 (2015).
[21] A. Deluca and Á. Corral, Acta Geophys. **61**, 1351 (2013).